

Auto-tuning of Deep Neural Networks by Conflicting Layer Removal

David Peer¹, Sebastian Stabinger, Antonio Rodríguez-Sánchez

Universität Innsbruck, Technikerstrasse 21a, 6020 Innsbruck, Austria

Abstract

Designing neural network architectures is a challenging task and knowing which specific layers of a model must be adapted to improve the performance is almost a mystery. In this paper, we introduce a novel methodology to identify layers that decrease the test accuracy of trained models. Conflicting layers are detected as early as the beginning of training. In the worst-case scenario, we prove that such a layer could lead to a network that cannot be trained at all. A theoretical analysis is provided on what is the origin of those layers that result in a lower overall network performance, which is complemented by our extensive empirical evaluation. More precisely, we identified those layers that worsen the performance because they would produce what we name *conflicting training bundles*. We will show that around 60% of the layers of trained residual networks can be completely removed from the architecture with no significant increase in the test-error. We will further present a novel neural-architecture-search (NAS) algorithm that identifies *conflicting* layers at the beginning of the training. Architectures found by our auto-tuning algorithm achieve competitive accuracy values when compared against more complex state-of-the-art architectures, while drastically reducing memory consumption and inference time for different computer vision tasks. The source code is available on <https://github.com/peerdavid/conflicting-bundles>

Keywords: Neural networks, Convolutional neural networks, conflicting bundles, neural architecture search (NAS), AutoML

1. Introduction

The training of deep neural networks is a complex and challenging task [1], one that can be achieved by better initialization strategies [2, 3], activation functions [4, 5], regularization methods [6, 7] and network architectures [8, 9, 10, 11]. It is known that the expressivity of the networks grows exponentially with depth [12, 13], but designing architectures that achieve high accuracy on a given task is challenging and can not only be achieved through the creation of deeper networks [11]. Figure 1 shows the accuracy of 176 different fully connected neural networks trained on MNIST at different

¹david.peer@outlook.com

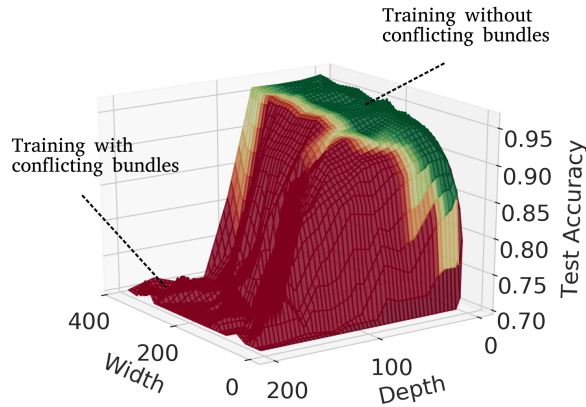


Figure 1: Test accuracy of 176 neural networks at different depths and widths trained on MNIST together with the boundary (yellow) that separates networks that induce conflicting training bundles (red) from those free of conflicting bundles (green).

depths and widths. We can observe that the optimal architecture w.r.t test accuracy that is trainable depends not only on depth, but also on a good balance between width and depth. Searching through different architectures in this manner in order to find a good configuration is not reasonable for real-world applications as too many possible configurations exist and the time required to train and evaluate each alternative is excessively long [14]. We will show theoretically and experimentally that *conflicting bundles* worsen the performance of neural network models. Models trained with conflicting bundles are shown in red in fig. 1, while the green color represents the models that are trained without conflicting bundles. The difference in accuracy values is quite noticeable. We will show that we are able to locate the layers that induce conflicting bundles already at the beginning of training, making our method an efficient strategy for dismissing underperforming architectures. The analysis and study of *conflicting bundles* we present in this paper will:

- Explain from a new theoretical perspective why a balance between width and depth is important, showing why residual connections help to train very deep networks.
- Help researchers to create more efficient state-of-the-art network architectures, which we will demonstrate by pruning as much as 60% of the layers of an already trained residual network without decreasing the accuracy significantly.
- Set the grounds for additional research pathways in Auto-ML

In this work, we further study the *conflicting training bundle problem*, as introduced in our previous work [15], providing a deeper theoretical analysis through a detailed derivation problem breakdown, which allows us to present an innovative methodology to prune residual networks. We will then provide additional experimental evaluation consisting of a lesion experiment, including a comparison to the work from Veit et al.

[16], which is later complemented with further evaluation on other residual connections than the identity mapping.

1.1. *The conflicting training bundle problem*

The output of a neural network is calculated by successively propagating inputs forward through all hidden layers. All output values of a layer are represented with finite resolution (e.g. 32 bit floating-point values). Consequently, two outputs that are only slightly different (less than the minimum resolution of the used floating-point representation), can become equal.

We have found that during training, weights were adjusted in wrong directions - leading to a worsened overall performance of the model - if any hidden layer produces the same output vector for two input examples with different labels. We call two samples *bundled* if the same output w.r.t. the floating-point resolution is produced for both inputs after passing through some hidden layer of the network. If both samples are labeled differently, we name them *conflicting*. We are able to determine the layer where the samples are bundled - called from now on, the *conflicting layer* - and therefore, non-optimal architectures can either manually or automatically be adapted to be more accurate and efficient as we will show in this paper.

1.2. *Outline*

In section 2, conflicting bundles are formally defined and their impact during training is analyzed. We show theoretically that the accuracy of a model is bound to decrease if conflicting bundles appear during training. In the worst-case scenario, the network will just not learn from data. In that same section, we introduce a novel metric to quantify and detect the precise layer that produces conflicting training bundles. In the experimental section 3, we will evaluate a broad range of different types of networks. Under controlled settings, we produce conflicting training bundles and study their effects per training epoch and layer. For completeness, fully connected networks, VGG nets, and ResNets are evaluated on different datasets. A detailed theoretical and empirical analysis is provided for residual connections which finally leads to a novel pruning method for ResNets that can be used to prune up to 60% of the layers from already trained ResNets without loss of accuracy. A novel NAS (neural-architecture-search) algorithm to tackle conflicting training bundles already at the beginning of the training is also introduced and compared against manually designed network architectures. A discussion and inspiration for future research are given in section 4.

1.3. *Related work*

Solving different optimization problems have been the subject of extensive study. LeCun et al. [17] has shown that a careful initialization of the weights of neural networks has a significant effect on the training process. Methods to initialize weights avoid vanishing information during forward-propagation and also avoid vanishing- or exploding gradients during backward propagation [2, 3, 1, 18, 19]. Very deep networks are difficult to optimize, even when variance-preserving initialization methods are used [10]. This problem can be overcome by highway networks from Srivastava et al. [10] that allow for the unimpeded information flow across several layers or residual learning

as presented by He et al. [8]. Historical developments and optimization problems that can occur during the training of neural networks are extensively described and summarized by the seminal survey of Schmidhuber [20] and the book by Goodfellow et al. [21].

To the best of our knowledge, we are the first to precisely locate and quantify the conflicting training bundles problem. The problem we have identified is related to, but different from, the Vanishing information problem [22]. They describe that information of original input patterns is lost in higher layers by going through multiple layer transformations and compressions. Kamimura and Takeuchi [22] also showed that convolutional neural networks do not suffer from this problem, probably due to the high dimensionality of hidden features. In the case of conflicting bundles, two different inputs are represented as equal when passing through a layer and, in contrast to the vanishing information problem, conflicting bundles also appear in convolutional networks. In the same domain of problems we find Shattered gradients [23], where the correlation between gradients in fully connected networks with L layers decay exponentially with $1/2^L$. The correlation decreases only with $1/\sqrt{L}$ if residual connections are used. Due to this fact, residual networks seem to be easier to train than fully connected networks. Shattered gradients are independent of the network’s width (theorem 1 of [23]). On the other hand, conflicting training bundles depend on both, depth and width as we will show later in this paper (section 3.3). Furthermore, conflicting bundles occur in very shallow networks, which rules out the vanishing- or exploding gradients problem [24]. Finally, different to the studies in the same domain of problems, where the focus is on mainly analyzing gradients during back-propagation, the analysis to discover conflicting bundles is performed during forward-propagation, which allows us to precisely detect the layer that introduces the problem.

2. Theoretical analysis

We will put our focus - for simplicity - on classification problems, although this analysis can be extended to regression problems. Let’s consider a training set $\mathcal{S} \in \mathcal{X} \times \mathcal{Y}$ that contains objects from a specific domain \mathcal{X} along with its labels \mathcal{Y} . Labels $y \in \mathcal{Y}$ are one-hot encoded and the dimensionality of the labels is N_c . If the input to a layer of a neural network is of dimension m and the output of dimension n , we use weight matrices $W \in \mathbb{R}^{n \times m}$ and bias terms $b \in \mathbb{R}^{n \times 1}$ to calculate the output. The output of a specific layer $l \in \{1, \dots, L\}$ for a network with L layers is a vector $a^{(l+1)}(x_i) = f(W^{(l)}a_i^{(l)} + b^{(l)})$ for some input $x_i \in \mathcal{X}$ and nonlinearity f . For simplicity, we will write $a_i^{(l+1)}$ instead of $a^{(l+1)}(x_i)$, where $a_i^1 = x_i$. Neural networks are trained using gradient descent with batches $\mathcal{B} \subseteq \mathcal{X}$. We assume without loss of generality that batches are uniformly distributed w.r.t. the class labels. The loss of the neural network for input x_i is calculated with $J_i = \text{CrossEntropy}(h_i, y_i)$, where $h_i = \text{softmax}(W^{(L)}a_i^{(L)} + b^{(L)})$. The gradient is calculated with $\frac{\partial J_i}{\partial W^{(L)}} = (h_i - y_i)a^{(L)T}$, which for a mini-batch \mathcal{B} would be $\frac{\partial J}{\partial W^{(L)}} = \frac{1}{|\mathcal{B}|} \sum_{i=1}^{|\mathcal{B}|} \frac{\partial J_i}{\partial W^{(L)}}$.

Two different input examples x_i and x_j are bundled, if the same output is produced for both inputs after the non-linearity of some hidden layer l is applied (the output layer

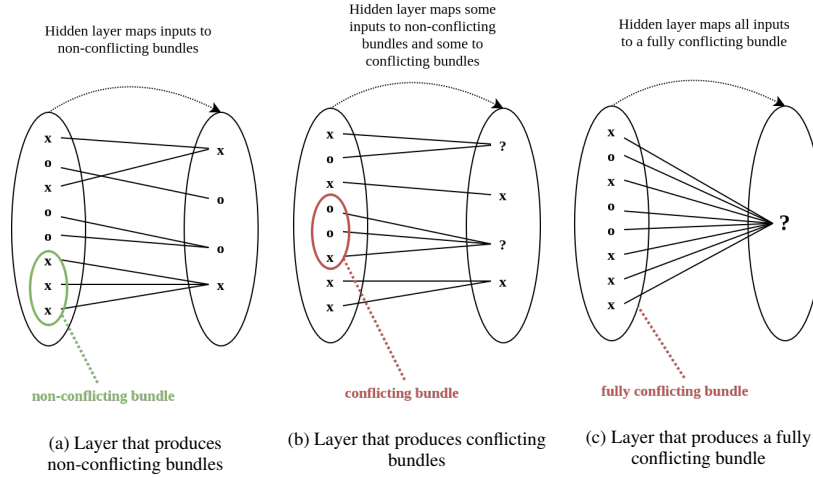


Figure 2: Graphical illustration of non-conflicting bundles (a) conflicting bundles (b) and a fully conflicting bundle (c) that are introduced by a hidden layer for inputs of two different classes (represented as 'x' and 'o').

is not included). This leads to the following definitions:

Definition 1. Two samples $x_i, x_j \in \mathcal{X}$ are *bundled* in layer l , if $a_i^{(l+1)} = a_j^{(l+1)}$ for the current configuration of learnable parameters.

Definition 2. Two samples $x_i, x_j \in \mathcal{X}$ are *conflicting*, if $y_i \neq y_j$ and there exists some layer $l \in \{1, \dots, L\}$ that bundles x_i and x_j . We call layer l the *conflicting layer* for x_i and x_j .

We next define the concept of a *bundle* and under which circumstances we call a bundle or a layer a *conflicting* one:

Definition 3. A *bundle* D_i^l contains all samples $x \in \mathcal{B}$ that are bundled after layer l and the set of all bundles $\mathcal{D}^l = \{D_1^l, D_2^l, \dots, D_k^l\}$ with $1 \leq k \leq |\mathcal{B}|$ ensure that $\forall i \neq j : D_i^l \cap D_j^l = \emptyset$ and $D_1^l \cup D_2^l, \dots, \cup D_k^l = \mathcal{B}$. A bundle that contains conflicting samples is called a *conflicting bundle*.

Definition 4. For the special case where all samples are bundled into a single bundle i.e. $\mathcal{D}^l = \{D^l\}$, we will call D_1^l a *fully conflicting bundle*.

By definition, a *conflicting bundle* contains at least two samples with different labels and a *fully conflicting bundle* contains all samples of a mini-batch and therefore all samples are conflicting. A graphical illustration is shown in fig. 2 to compare non-conflicting bundles, conflicting-bundles and fully-conflicting bundles. We will now make use of the definitions to derive the negative effects that arise when neural networks are trained with fully conflicting bundles or conflicting bundles in general.

2.1. Fully conflicting bundle

First, we will evaluate the gradient w.r.t. $W^{(L)}$ assuming that a fully conflicting bundle (definition 4) occurs during training:

$$\begin{aligned}
 \frac{\partial J}{\partial W^{(L)}} &= \frac{1}{|\mathcal{B}|} \sum_{i=1}^{|\mathcal{B}|} \frac{\partial J_i}{\partial W^{(L)}} \\
 &= \frac{1}{|\mathcal{B}|} \sum_{i=1}^{|\mathcal{B}|} (h_i - y_i) a_i^{(L)T} && \text{Mini-batch gradient} \\
 &= \frac{1}{|\mathcal{B}|} \sum_{i=1}^{|\mathcal{B}|} (h - y_i) a^{(L)T} && \text{Fully conflicting bundle assumption} \\
 &= \frac{1}{|\mathcal{B}|} \left(|\mathcal{B}|h - \sum_{i=1}^{|\mathcal{B}|} y_i \right) a^{(L)T} \\
 &= \frac{1}{|\mathcal{B}|} \left(|\mathcal{B}|h - \frac{|\mathcal{B}|}{N_c} \mathbf{1} \right) a^{(L)T} && \text{Uniform batches assumption} \\
 &= \left(h - \frac{1}{N_c} \mathbf{1} \right) a^{(L)T}
 \end{aligned}$$

where $\mathbf{1}$ is a vector of dimension $N_c \times 1$ with unitary elements. First of all, we can see that all h_i are collapsed into a single h , which is the fully conflicting bundle assumption. All labels can also be collapsed into a single $\mathbf{1}$ vector scaled by $|\mathcal{B}|/N_c$ since we assumed uniformly distributed batches. The first observation is that the labels y_i disappeared from the gradient, i.e. the gradient is uncorrelated of y_i and therefore we conclude that the network cannot learn from data. Please note that this is different from shattered gradients [23], where gradients become uncorrelated from its input x_i (and not y_i). Another observation is that the gradient becomes zero whenever all components of h are equal to $1/N_c$ and therefore we hypothesize:

Hypothesis 1. If a fully conflicting bundle occurs anywhere in the hierarchy of a neural network during training, all labels are ignored and weights are adjusted until each output neuron fires with constant value $\frac{1}{N_c}$.

Note that the value of each neuron becomes $\frac{1}{N_c}$ because we assumed equally distributed labels in the batches. If we relax this assumption, each neuron will fire with a constant value that represents the imbalance of the dataset. For example, if 75% of the examples are of class one, the corresponding neuron will fire with a constant value of 0.75.

2.2. Conflicting bundles

We now relax the assumption that a *fully* conflicting bundle occurs and study the gradient for the case where some conflicting bundles occur (see definition 3):

$$\begin{aligned}
 \frac{\partial J}{\partial W^{(L)}} &= \frac{1}{|\mathcal{B}|} \sum_{i=1}^{|\mathcal{B}|} \frac{\partial J_i}{\partial W^{(L)}} \\
 &= \frac{1}{|\mathcal{B}|} \sum_{i=1}^{|\mathcal{B}|} (h_i - y_i) a_i^{(L)T} && \text{Mini-batch gradient} \\
 &= \frac{1}{|\mathcal{B}|} \sum_{D \in \mathcal{D}^L} \left(|D| h_D - \sum_{i=1}^{|D|} y_i \right) a_D^{(L)T} && \text{Conflicting bundles assumption}
 \end{aligned}$$

Compared to the fully conflicting bundle case, where labels disappeared, labels in this case are included in the calculation of the gradient. Unfortunately, for the same output h_D different labels are grouped by $\sum_{i=1}^{|D|} y_i$. We can then think of the effect of conflicting bundles as being similar to the effect of noisy labels, for which it is well known that the model performance is worsened [25]. This leads us to the following hypothesis that will be confirmed in the experimental section 3:

Hypothesis 2. If conflicting bundles occur anywhere in the hierarchy of a neural network during training, the accuracy of the trained model is worsened.

To check the correctness of hypothesis 1 and hypothesis 2, we have to be able to detect situations where conflicting bundles occur and measure the degree of conflict of a bundle. A metric to quantify conflicting bundles is introduced next.

2.3. Conflicting bundle metric

To measure whether two samples x_i and x_j are bundled at layer l we must check if $a_i^{(l+1)} = a_j^{(l+1)}$ (definition 1). The finite resolution of floating point values must be considered. It then makes a difference whether the vectors are used during forward- or backpropagation: During backpropagation, a_i vectors are scaled by the learning rate α and $1/|\mathcal{B}|$ before they are subtracted from the weights. Therefore, it is possible that very small values that are different during forward propagation are bundled during backpropagation due to the finite resolution of floating-point values. To consider this situation, we approximate definition 1 with

$$\frac{\alpha}{|\mathcal{B}|} \|a_i^{(l+1)} - a_j^{(l+1)}\|_{\infty} \leq res(W^l) \tag{1}$$

where $res(W^l)$ is the smallest possible resolution that is supported by the floating-point representation w.r.t the weights W^l of the GPU or CPU at hand. Note that eq. (1) depends only on the output of the layer such that this metric can be used for any type of layers, i.e. fully connected, convolutional, pooling or others.

A bundle D_i^l (definition 3) is then the set of all vectors that are equal accordingly to eq. (1). We are mainly interested in *conflicting* bundles and our aim is to quantify how conflicting a single bundle $D_i \in \mathcal{D}^l$ at training step t and layer l is. A standard measure fitted for this task is to evaluate the entropy $H^l(t, D_i)$ as:

$$H^l(t, D_i) = - \sum_{n=1}^{N_c} p(n) \ln(p(n) + \epsilon) \quad (2)$$

where $p(n)$ represents the probability that samples of class n occur in bundle D_i and ϵ is an arbitrarily small value ensuring numerical stability. The value of entropy $H^l(t, D_i)$ is large if the bundle D_i created in layer l contains many examples with different labels. Otherwise, if a small number of examples share the same label, $H^l(t, D_i)$ is accordingly small.

To measure the entropy of all bundles, the size of each bundle must also be considered, because a large conflicting bundle D_1 affects the training more than a small conflicting bundle D_2 . Therefore, we consider the bundle size of each bundle in order to provide a *bundle entropy at training step t for layer l* through:

$$H^l(t) = \frac{1}{|\mathcal{B}|} \sum_{D_i \in \mathcal{D}^l} |D_i| \cdot H(t, D_i) \quad (3)$$

If only one sample or samples of the same class are included in a bundle, $H^l(t)$ is zero. If a fully conflicting bundle occurs then $H^L = \ln(N_c)$.

To be able to check the correctness of hypothesis 1 and hypothesis 2, we must determine whether conflicts occur during training. Therefore, we evaluate $H^l(t)$ after multiple time steps and report an average value of the bundle entropy that occurred during training. We call this metric the *bundle entropy H^l* . Unless otherwise specified, we will use H^l for the bundle entropy of the last hidden layer L . It is important to mention that the bundle entropy $H^L > 0$ iff at least two samples with different labels are bundled during training.

3. Experimental evaluation

In section 2 we hypothesized that if conflicts occur, the test loss increases (hypothesis 2) and in the extreme case all labels would be ignored (hypothesis 1). In this section, we evaluate whether conflicting bundles occur and their effect during the training of state-of-the-art methods.

3.1. Setup

We believe that the analysis of conflicting bundles can lead to new methods by avoiding the negative effects of conflicting layers. The focus of this paper is therefore not to fine-tune specific state-of-the-art methods but to shed light on this problem. We will consider the following setup for evaluation:

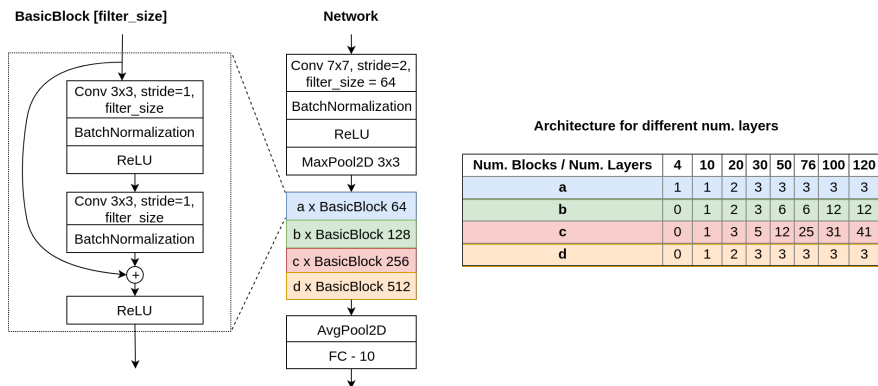


Figure 3: ResNet architecture He et al. [8] used in our experimental evaluation.

Training. We will use the term "fully connected networks" - or equivalently "FC-Net" - for networks that are built only with fully connected layers: For networks, such as the ones introduced by He et al. [8] and as shown in fig. 3, the term we will use is "residual neural networks" or "ResNet" in short; and for the same type but without residual connections, "VGG-Net". We will use the most commonly-used datasets [26, 27, 28, 29] and random data augmentation to evaluate conflicting bundles under a standard setup as follows: We normalize and randomly crop, flip (except for MNIST), and adapt the brightness of images; ReLU activations are used and therefore weights are initialized with the HE initializer [3] to avoid vanishing or exploding gradients; To minimize the cross-entropy loss we use the state-of-the-art optimizer Ranger (RAdam [30] + Lookahead [31]) with a mini-batch size of 64, a learning rate of 0.001 and weight decay of 0.01. ResNets and VGG-Nets are trained for 120 epochs and the FC-Nets for 50 epochs. The source code is implemented in TensorFlow Version 2.2.0 [32] and available for download on GitHub². Training is executed on a multi-GPU cluster, where one GPU is used to measure conflicting bundles. All experiments are also implemented and designed to be executable on smaller systems with a single GPU.

Evaluation. Test accuracy is averaged over the last 5 epochs in order to exclude outliers. We estimate conflicting bundles through a random subset of the training set $\mathcal{B} \subseteq \mathcal{X}$ with $|\mathcal{B}| = 2048$ to speed up computations and we found empirically that this number of samples is large enough to represent the bundle entropy. To calculate bundles, we created a vectorized function that iterates only once overall $x \in \mathcal{B}$ such that this calculation can also be done on small hardware setups with e.g. only one GPU. Therefore, the complexity to evaluate all layers is $O(|\mathcal{B}| \times L)$. Please note that examples of the training data and not the test data are used to measure conflicting training bundles, as those examples are used to adjust the weights of the network. The developed TensorFlow software module to evaluate conflicting bundles is certified for

²<https://github.com/peerdavid/conflicting-bundles>

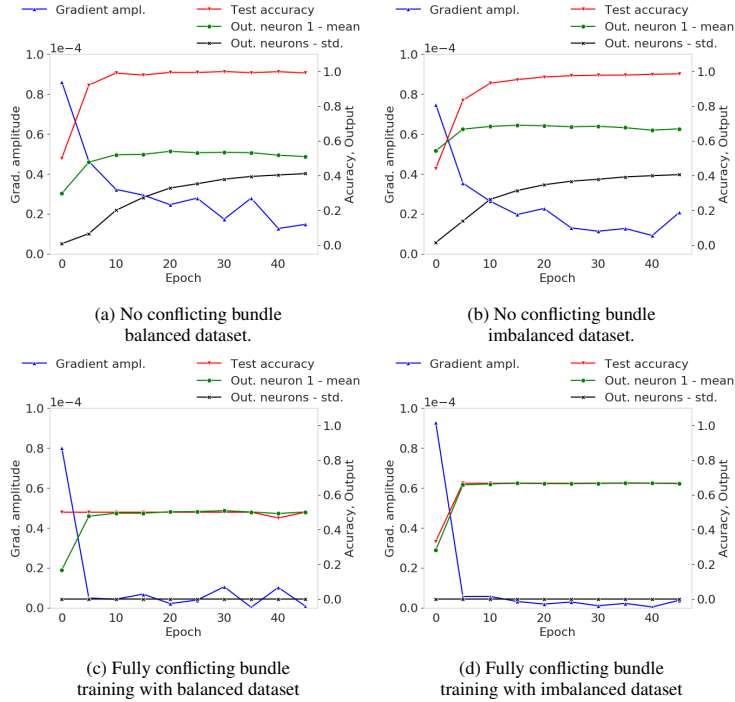


Figure 4: Results using a toy dataset and manually initialized weights with the absence conflicting bundles for (a) balanced and (b) imbalanced datasets. Compare with (c) and (d) in the presence of a fully conflicting bundle. The gradient (blue line), test accuracy (red line), mean of output neuron 1 (green line) and standard deviation of output neurons (black line) are shown.

computational reproducibility³ and is documented in detail in our previous work [33].

3.2. Training with a fully conflicting bundle

We will first evaluate if training with fully conflicting bundles settles at a region where all neurons fire with a constant value as predicted in hypothesis 1. For this, we will compare the training of a neural network with and without a fully conflicting bundle under controlled settings. The fully conflicting bundle is produced in a setup where the conditions can be tightly controlled through manual weight initialization. In this first experiment, we use a toy dataset with two classes (class zero if $x_i < 0.5$, class one otherwise) and 1,000 training examples for a two-layer (two neurons per layer) network with ReLU activation followed by softmax and cross-entropy loss function.

As fig. 4a shows, this simple network can solve the problem with a training accuracy of ≈ 1.0 if weights are initialized such that no conflicting bundle is produced. Compare those results with the graph shown in fig. 4c, where we initialized weights such that a fully conflicting bundle is produced. It can be seen that for this weight

³<https://codeocean.com/capsule/8314999/tree/v1>

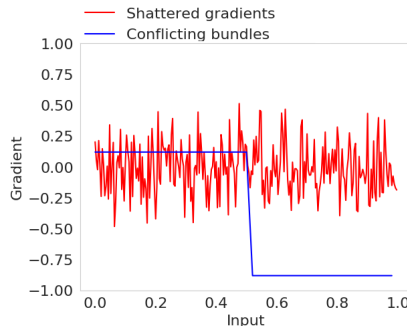


Figure 5: White noise of shattered gradients [23] (red line) compared with the gradients of the conflicting training bundle problem (blue line).

configuration each output neuron fires with a constant value of $1/N_c = 0.5$ after 50 epochs as predicted by hypothesis 1. In fig. 4b and fig. 4d the network is trained with an imbalanced dataset such that 66% of the training examples are of class zero and 33% are of class one. We can see in fig. 4b that each neuron reflects the aforementioned imbalance (section 2.1) of the dataset since neuron one fires with a constant value of 0.66.

The gradient (blue line) of the training without conflicting bundles (fig. 4a and 4b) and with fully conflicting bundles (fig. 4c and 4d) is similar at the beginning of the training process, ruling out the gradient vanishing or exploding problem. Also, as networks have only two layers, this problem would by principle not arise. For completeness in excluding we are facing a case of the shattered gradient problem, we further analyzed these results by analyzing white noise in both cases (shattered gradients and conflicting bundles), that is, we evaluated whether inputs and their respective gradients are uncorrelated. If they were, it would indicate that we are facing a case of the shattered gradient problem [23]. As shown in fig. 5, the conflicting bundles and the shattered gradients problems are of different nature since the gradients of conflicting bundles are highly correlated with its input as opposed to the case of shattered gradients.

3.3. Fully connected networks

The test accuracy of more than a hundred FC-Nets networks together with the conflicting boundary was already introduced in fig. 1. In this section, we study the bundle entropy and the number of bundles that occur during training in more detail by analyzing each training epoch and each layer of different FC-Nets trained on MNIST. Results are shown in fig. 6 and fig. 7.

Figure 6a shows the training of two networks (25 layers) with widths of 10 and 25. The number of conflicts increases as we go higher in the hierarchy of the network, indicating that subsequent layers cannot fully solve conflicts. We can then conclude that the number of conflicting training bundles increases as the depth of the network increases. If we are to compare the results of width 10 with those of width 25, fig. 6a shows that conflicts occur much earlier in the architecture if the dimensionality of hidden features

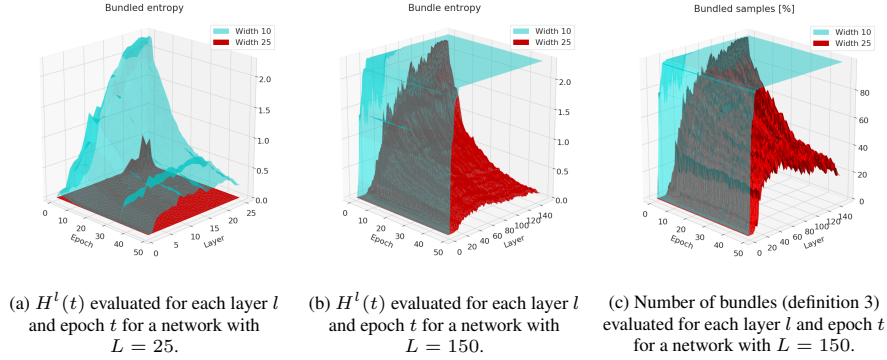


Figure 6: Evaluation of FC-Nets at different L depths and two widths (10 and 25) w.r.t conflicting training bundles.

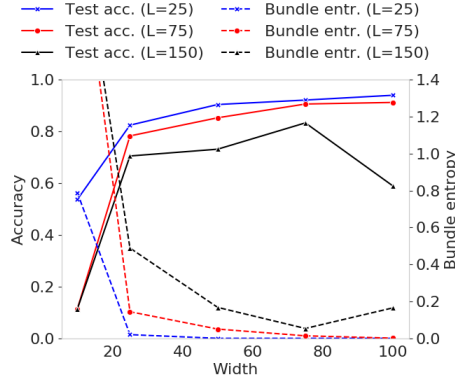


Figure 7: Test accuracy (solid lines) and bundle entropy H^L (dotted lines) for FC-Nets with different depths (L) and widths.

is smaller. This would explain the test-accuracy pattern shown in fig. 1, where the yellow boundary was created - already at the beginning of training - by observing that if conflicting bundles occur during training, conflicts can only be slowly resolved as training proceeds. Two deeper networks with 150 layers are analyzed in fig. 6b and fig. 6c. For both widths (10 and 25), conflicting bundles occur during training, but for a width of 10 it can be seen that a fully conflicting bundle occurs since $H^l(t) \approx 2.3$. Conflicts were never resolved, which was confirmed by the accuracy being not better than chance (hypothesis 1). Interestingly, if we compare fig. 6a and fig. 6b, we can conclude that for a fixed width, the position of the layer where conflicting bundles occur is similar among networks with different depths. For example, the first conflicting layer for width 25 is layer 19 for both depths, $L = 25$ and $L = 150$. Therefore, it would be sufficient to only evaluate the deepest network to find the conflicting boundary (fig. 1).

The correlation of the bundle entropy and test accuracy is evaluated in fig. 7, which shows that the bundle entropy H^L is negatively correlated with the test accuracy. This

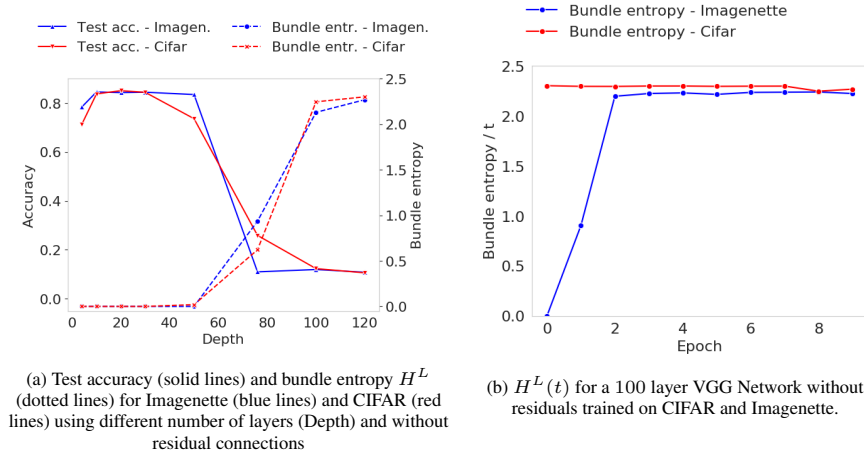


Figure 8: Performance and bundle entropy of VGG-Nets trained on CIFAR and Imagenette.

further supports hypothesis 2, which stated that conflicting bundles worsen the test accuracy of neural networks. One natural question that arises from the experimental evaluation in this section is whether conflicts also occur for computer vision tasks and convolutional layers because hidden features are high dimensional, which we will analyze next.

3.4. VGG-Nets

We evaluate next hypothesis 1 and hypothesis 2 experimentally on several VGG-Nets for different datasets. Figure 8 shows the performance and bundle entropy for Imagenette and CIFAR (blue and red lines respectively in fig. 8a). Figure 8b shows the bundle entropy at each time step $H^L(t)$ for a network with 100 layers trained on Imagenette.

As fig. 8a) shows, for small networks with only four layers, the model suffers from underfitting and therefore the test accuracy is 71% for CIFAR and 78% for Imagenette. From 10 to 40 layers, the test accuracy is quite higher and the bundle entropy is zero, which indicates no conflicting bundles during training. After 40 and 60 layers for CIFAR and Imagenette respectively, the bundle entropy H^L increases proportional to depth. From this point, the test accuracy decreases proportional to the increase in bundle entropy (hypothesis 2). For 120 layers, the entropy is at a peak for 10 classes, i.e. ≈ 2.3 , which indicates a fully conflicting bundle. In this case, the accuracy is also not better than chance (hypothesis 1) as shown in fig. 8a). Previous work has already reported a drop in test accuracy when training very deep convolutional networks [23, 8, 10]. This behavior can be the result of the appearance of conflicting bundles. If we analyze the progress of training (fig. 8b), it can be seen that conflicting bundles appear after just a few epochs of training. Even though it is well known that a proper weight initialization is critical for a successful training process, these results show that even when weights are initialized correctly, the probability for conflicting layers increases

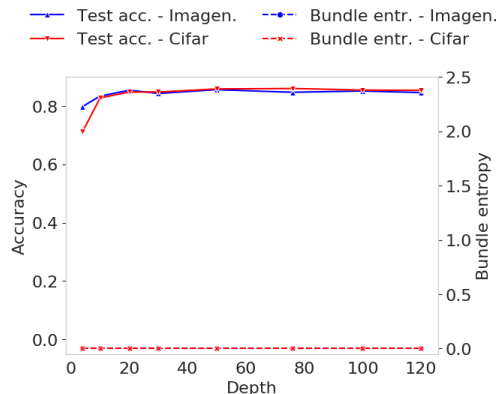


Figure 9: Test accuracy and bundle entropy H^L for different number of layers with residual connections

proportionally with each layer added to the architecture (including the case of very high dimensional features such as images).

It is well known that residual connections reduce the shattered gradient problem. In section 3.2 and section 3.3 we showed that that shattered gradients problem is different from conflicting bundles. We analyze next whether residual connections help also at mitigating the conflicting bundles problem.

3.5. Residual neural networks

To evaluate whether residual networks also suffer from conflicting bundles, we trained ResNets with different depths on different datasets. Figure 9 shows that the bundle entropy is zero for all network depths and datasets, this would indicate that conflicts are solved by residual connections and therefore, the training of very deep convolutional networks is possible with an accuracy similar to all the different residual networks (hypothesis 2). He et al. [8] already showed that residual networks are easier to optimize, our conflicting bundle analysis provides a new explanation on why that seems to be the case.

We next evaluated each network block by measuring whether conflicts occur directly after the second batch normalization layer and before the residual connection is added. We found that many blocks ($\approx 60\%$ in a ResNet-120 trained on CIFAR) exist where conflicts are produced directly after the second batch normalization layer. The conflicts seem to be resolved after the residual connection is added to this otherwise conflicting output. For the sake of completeness, we provide an analysis from a theoretical point of view: Let's consider layer l as the one producing conflicts for x_i and x_j in the absence of residual connections. We will call this as the intermediate conflicting output $d^{(l)}$ (which is the same for x_i and x_j as it is assumed to be conflicting). The output for inputs x_i and x_j of the layer which adds a residual connection $r^{(l)}(x)$ is $a^{(l+1)}(x) = r^{(l)}(x) + d^{(l)}$. The residual $r^{(l)}(x)$ is the identity mapping [8] and therefore it can be shown that the function $a^{(l+1)}(x)$ is bijective for inputs x_i and x_j . Definition 1 is violated because $a_i^{(l+1)} \neq a_j^{(l+1)}$ and the conflict is resolved as shown

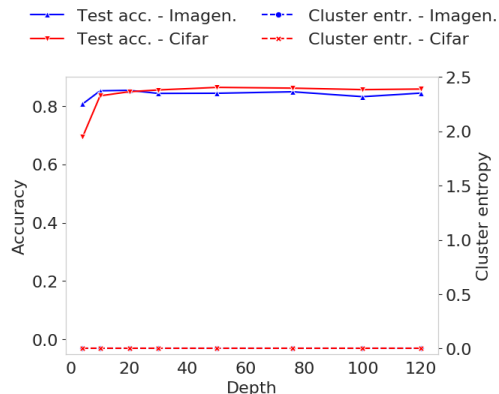
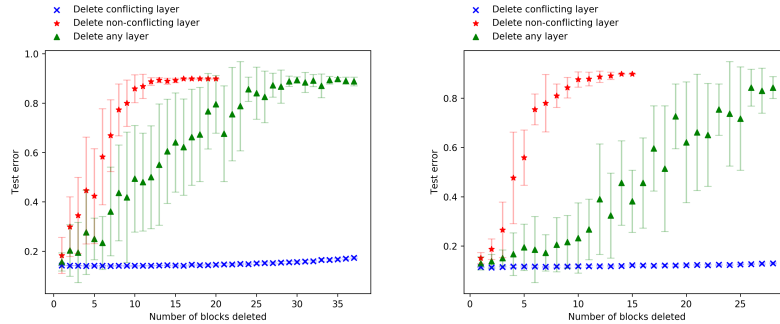


Figure 10: A network that uses the residual function $r^{(l)}(x) = 2x + 0.1$

empirically.

This analysis also holds without the assumption that the residual connection is the identity function as any bijective residual function $r^{(l)}(x)$ is sufficient in order to solve conflicts, which has already been extensively studied by He et al. [34]. To further confirm this fact, we executed an additional experiment where we trained a residual network on Imagenette with the mapping function $r^l(x) = 2x + 0.1$ to evaluate if a) produces a similar accuracy and, b) it also solves conflicts. Figure 10 shows the results of this experiment. Therefore, our theory extends preliminary work [35] that explicitly states that their theoretical investigation holds only for residuals with identity mappings.

Another important fact from this theoretical analysis is, that conflicting layers that are bypassed with residual connections represent only a linear mapping, because $a^{(l+1)}(x) = r^{(l)}(x) + d^{(l)}$. Therefore, it should be possible to completely delete layers that produce conflicts within a residual block from already trained residual networks with only a minor impact on the test-error. Veit et al. [16] has already shown that in fact the test-error increases only slightly as more and more layers are deleted from the architecture of trained residual networks. We reproduced those results and additionally evaluate separately how the error increases if (1) we delete conflicting layers or (2) we delete non-conflicting layers. Results of our lesion study are shown in fig. 11. It can be seen that more than in fact, 60% of the layers for a Resnet-120 trained on CIFAR and more than 50% when trained on Imagenette can be removed, having a minor effect on the test error (blue crosses in fig. 11). This is true only when we delete conflicting and partially-conflicting layers. Otherwise, if non-conflicting layers are deleted from the architecture we can see that the error rises abruptly (red stars in fig. 11). On the other hand, if we remove random layers from the architecture (green triangles in fig. 11), this rise is not so abrupt but we still observe a large steady rise in the test error. This behavior makes us believe that this latter error increase may not be only due to the fact that ResNets may behave like ensembles of shallow networks [16], but also to that a combination of conflicting and non-conflicting layers are dropped from the architec-



(a) Performance of ResNet-120 trained for 120 epochs on CIFAR. n blocks (with two layers per block) are deleted of the trained network. (b) Performance of ResNet-120 trained for 120 epochs on Imagenette. n blocks (with two layers per block) are deleted of the trained network.

Figure 11: Lesion studies for a trained ResNet-120. We compare lesions of conflicting-layers, non-conflicting layers and any layer following Veit et al. [16] and report the mean and the standard deviation of 15 executions.

ture (the former having no effect on performance, the latter having a large effect as shown by the red stars). This statement would be further supported by looking at the standard-deviation values, being much larger when random layers are deleted from the architecture when compared to the other two cases (especially when conflicting layers are removed).

Instead of training those networks and pruning them after the training, it would be of much more interest for the sake of efficiency to have at our disposal a pruning algorithm that removes those conflicting layers already at the beginning of the training.

3.6. Auto-tuning the depth of a network

The *conflicting bundle auto-tune* (CBA-tune) pruning algorithm that we will present here looks first for the conflicting boundary - e.g. the yellow border from fig. 1 - for a given input dimensionality. Afterwards, it will iteratively prune the network to ensure that no conflicting bundles occur during training. The pseudocode for CBA-tune is shown in algorithm 1 and works as follows: First, the requested network would be trained for at least one epoch, e.g. the one from section 3.4 with 120 layers. Then, the first conflicting layer l with $H^l(t) > 0$ and all subsequent layers of the same block type (as specified in [8]) are removed from the architecture (section 3.3). A side effect of this pruning is that also the dimensionality between two layers changes and therefore, we need to restart the training with the new pruned architecture rather than continuing the training to avoid dimensionality problems. We then re-initialize all weights with the HE initializer [3], because the network is trained for one epoch with conflicting bundles such that weights of the network are adjusted into wrong directions. This process is repeated until no conflicting layer can be found and the network is successfully trained for 120 epochs.

As an example, we will explain here the process followed for the network used in section 3.4 with 120 layers. In order to show the validity of our CBA-tune approach, we will compare the pruned network found by the auto-tune algorithm with the ResNet

Algorithm 1 CBA-tune

```
1: model  $\leftarrow$  VGG-Net with  $a = 3, b = 12, c = 41, d = 3$   $\triangleright$  Initially create the
   largest VGG-Net with 120 layers.
2: Initialize weights of model  $\triangleright$  The HE-Initializer [3] is used to initialize weights.
3:  $i \leftarrow 0$ 
4:
5: while  $i < 120$  do
6:   Train model for one epoch
7:    $i \leftarrow i + 1$ 
8:
9:   if Conflicting bundles occurred during training then
10:     $l \leftarrow$  First conflicting layer w.r.t block-type  $\triangleright 0 < l < 120$ 
11:     $t \leftarrow$  Block-type of layer  $l$   $\triangleright t \in \{a, b, c, d\}$ 
12:    Prune block-type  $t$  of the current model to size  $l$   $\triangleright$  Prune only one
       block-type per iteration.
13:    Initialize weights of model
14:     $i \leftarrow 0$ 
15:   end if
16: end while
```

Table 1: Comparison of test accuracy, memory consumption (based on checkpoint size) and inference time.

Dataset	Name	Layers	Accuracy [%]	Mem. [MB]	Time / Step [ms]
Imagenette	ResNet	50	85.6 ± 0.8	116	310
	Auto-tune	24 ± 1.6	84.7 ± 0.1	63 ± 6.0	200 ± 0.0
Cifar	ResNet	76	85.7 ± 0.4	178	130
	Auto-tune	19 ± 0.9	85.3 ± 0.4	53 ± 1.0	48 ± 2.5
Svhn	ResNet	50	95.4 ± 0.1	116	90
	Auto-tune	19 ± 0.9	95.1 ± 0.1	54 ± 0.5	46 ± 1.8
Mnist	ResNet	50	99.4 ± 0.0	116	88
	Auto-tune	17 ± 1	99.3 ± 0.5	54 ± 2.1	40 ± 0.0

that produced the highest accuracy (ResNet-50 as in section 3.5). In addition to the CIFAR and Imagenette datasets, we evaluated the SVHN [29] and MNIST [28] datasets for completeness. Each experiment is run three times and we report the mean and standard deviation. Table 1 shows that the different architectures found by our CBA-tune algorithm differ only slightly between different runs as shown in table 3. Our CBA-tune algorithm changed the architecture at most three times before the final pruned network was found and the architecture was changed after the first and before the second epoch. As an example, the evolution for one execution of CBA-tune algorithm trained on CIFAR is shown in table 2. Our automatic depth selection process is computationally very efficient as it took only three epochs of training to find the conflict-free architecture. The number of layers found by the CBA-tune algorithm is within the optimal region w.r.t. test accuracy (fig. 8a) and the depth increases proportional to its input dimensionality (section 3.3). The number of layers obtained by CBA-tune also corresponds to the

Table 2: Evolution of the architecture as created by CBA-tune shown for Cifar. The numbers show how many basic blocks (as shown in fig. 3, left side) are still used after the pruning was executed.

Epoch	Block a	Block b	Block c	Block d
Start	3	12	41	3
1	3	4	41	3
2	3	3	41	3
3	3	3	0	3

Table 3: Three different executions of CBA-tune together with the corresponding architecture that was used for training.

Dataset	Run	Layers	Block				Accuracy [%]	Mem. [MB]	Time [ms]
			a	b	c	d			
Imagenette	1	26	3	3	3	3	84.5	69	200
	2	22	3	4	0	3	84.7	55	200
	3	24	3	3	2	3	84.8	65	200
Cifar	1	20	3	3	0	3	85.3	54	50
	2	18	3	2	0	3	84.9	53	45
	3	20	3	3	0	3	85.8	53	50
Svhn	1	20	3	3	0	3	95.3	54	47
	2	20	3	3	0	3	95.1	54	47
	3	18	3	2	0	3	95.0	53	43
Mnist	1	18	3	1	1	3	99.2	57	40
	2	16	3	1	0	3	99.3	52	40
	3	16	3	1	0	3	99.3	52	40

ones presented by Veit et al. [16], that is, paths in ResNets are just between 10 to 34 layers deep. Table 1 further shows that the test accuracy of the networks with conflicting layers removed is not only comparable to their residual counterpart, but also the inference time and the memory consumption is drastically reduced since fewer layers are used.

4. Discussion and future work

In this paper, we defined and introduced the problem of *conflicting training bundles*. In section 2 this problem is analyzed theoretically and we hypothesized that (1) conflicting bundles that occur during training decrease the accuracy of trained models (hypothesis 2) and (2) fully conflicting bundles can lead to networks that cannot be trained at all (hypothesis 1). In the experimental section 3 both hypotheses were evaluated empirically on many different hyperparameters, architectures, and datasets. We first defined a toy dataset under controlled settings to be able to analyze the behavior of neural networks. Later, we showed empirically for Fully connected networks trained on MNIST that the number of conflicting training bundles increases proportional to (1) the depth of the network and (2) a decreasing dimensionality of hidden features. We have also shown that conflicts occur early in the training and that the bundle entropy is negatively correlated with the accuracy of the trained model. Our findings showed

that conflicting bundles do not shatter gradients, or in other words, the shattering gradients problem [23] is different from the conflicting bundles problem presented here. VGG-Nets were then evaluated in section 3.4 to confirm that conflicting-bundles can also occur when hidden features are very high-dimensional, as it is the case for images. Conflicting layers can be bypassed with residual connections, and we proved that any bijective residual connection can be used, not only the identity function [8, 34, 35]. Conflicting layers that are bypassed with residuals produce a linear mapping between its input and its output. We could easily remove those layers from already trained networks, such that as much as 60% of the layers of a residual network could be removed without increasing the accuracy which is an alternative explanation to the idea that residual networks behave like ensembles of shallow networks [16]. The CBA-tune we have presented in this work automatically prunes VGG-Nets to avoid conflicting layers as early as at the beginning of the training. With this computationally efficient algorithm, the accuracy of the network models was maintained while the computational power and memory consumption was drastically reduced.

The findings and insights of this paper can be of great help for future AutoML methods. For example, mutated architectures can be rejected after a few training steps in evolutionary algorithms if conflicting bundles occur following hypothesis 2. Additionally, architectures can be precisely adapted because the layer(s) causing conflict(s) could be known. We believe that the analysis of conflicting bundles will help future researchers to design better deep neural network architectures. In this paper, we pruned the depth of the network to avoid conflicting layers. In future work, it would be interesting to also explore alongside other dimensions of the hyperparameter space such as the learning-rate, the batch-size, or the width of the network. The presented work has shown that residuals force a linear mapping between its input and its outputs and therefore those layers can also be removed as we demonstrated in our lesion experiment, which could lead to future studies that could transform conflicting layers into layers not containing conflicts.

Acknowledgments

We acknowledge all members of the IIS research group, the European Union’s Horizon 2020 program for the grant agreement no. 731761 (IMAGINE) and Deep-Opinion for the opportunity to continue with this research in the future.

References

- [1] G. E. Hinton, S. Osindero, Y. W. Teh, A fast learning algorithm for deep belief nets, *Neural Computation* 18 (2006) 1527–1554.
- [2] X. Glorot, Y. Bengio, Understanding the difficulty of training deep feedforward neural networks, in: Y. W. Teh, M. Titterton (Eds.), *Proceedings of the Thirteenth International Conference on Artificial Intelligence and Statistics*, volume 9 of *Proceedings of Machine Learning Research*, PMLR, Chia Laguna Resort, Sardinia, Italy, 2010, pp. 249–256. URL: <http://proceedings.mlr.press/v9/glorot10a.html>.

- [3] K. He, X. Zhang, S. Ren, J. Sun, Delving deep into rectifiers: Surpassing human-level performance on imagenet classification, in: 2015 IEEE International Conference on Computer Vision (ICCV), 2015, pp. 1026–1034. doi:10.1109/ICCV.2015.123.
- [4] G. E. Dahl, T. N. Sainath, G. E. Hinton, Improving deep neural networks for lvsr using rectified linear units and dropout, in: 2013 IEEE International Conference on Acoustics, Speech and Signal Processing, 2013, pp. 8609–8613.
- [5] D. Misra, Mish: A self regularized non-monotonic neural activation function., CoRR abs/1908.08681 (2019).
- [6] S. Ioffe, C. Szegedy, Batch normalization: Accelerating deep network training by reducing internal covariate shift, in: F. Bach, D. Blei (Eds.), Proceedings of the 32nd International Conference on Machine Learning, volume 37 of *Proceedings of Machine Learning Research*, PMLR, Lille, France, 2015, pp. 448–456. URL: <http://proceedings.mlr.press/v37/ioffe15.html>.
- [7] N. Srivastava, G. Hinton, A. Krizhevsky, I. Sutskever, R. Salakhutdinov, Dropout: a simple way to prevent neural networks from overfitting, *The journal of machine learning research* 15 (2014) 1929–1958.
- [8] K. He, X. Zhang, S. Ren, J. Sun, Deep residual learning for image recognition, in: Proceedings of the IEEE conference on computer vision and pattern recognition, 2016, pp. 770–778.
- [9] D. Peer, S. Stabinger, A. Rodriguez-Sanchez, Increasing the adversarial robustness and explainability of capsule networks with γ -capsules, 2018. arXiv:1812.09707.
- [10] R. K. Srivastava, K. Greff, J. Schmidhuber, Highway networks, *Deep Learning Workshop, International Conference on Machine Learning (2015)*.
- [11] M. Tan, Q. V. Le, Efficientnet: Rethinking model scaling for convolutional neural networks, in: Proceedings of the 36nd International Conference on Machine Learning, 2019.
- [12] D. Peer, S. Stabinger, A. Rodríguez-Sánchez, Limitation of capsule networks, *Pattern Recognition Letters* 144 (2021) 68–74.
- [13] M. Raghu, B. Poole, J. Kleinberg, S. Ganguli, J. Sohl-Dickstein, On the expressive power of deep neural networks, in: international conference on machine learning, PMLR, 2017, pp. 2847–2854.
- [14] D. Stathakis, How many hidden layers and nodes?, *International Journal of Remote Sensing* 30 (2009) 2133–2147.
- [15] D. Peer, S. Stabinger, A. Rodríguez-Sánchez, Conflicting bundles: Adapting architectures towards the improved training of deep neural networks, in: Proceedings of the IEEE/CVF Winter Conference on Applications of Computer Vision, 2021, pp. 256–265.

- [16] A. Veit, M. J. Wilber, S. Belongie, Residual networks behave like ensembles of relatively shallow networks, in: *Advances in neural information processing systems*, 2016, pp. 550–558.
- [17] Y. A. LeCun, L. Bottou, G. B. Orr, K.-R. Müller, Efficient backprop, in: *Neural networks: Tricks of the trade*, Springer, 2012, pp. 9–48.
- [18] P. Krähenbühl, C. Doersch, J. Donahue, T. Darrell, Data-dependent initializations of convolutional neural networks., in: Y. Bengio, Y. LeCun (Eds.), *ICLR (Poster)*, 2016.
- [19] D. Mishkin, J. Matas, All you need is a good init., in: Y. Bengio, Y. LeCun (Eds.), *ICLR (Poster)*, 2016.
- [20] J. Schmidhuber, Deep learning in neural networks: An overview, *Neural networks* 61 (2015) 85–117.
- [21] I. Goodfellow, Y. Bengio, A. Courville, *Deep learning*, MIT press, 2016.
- [22] R. Kamimura, H. Takeuchi, Sparse semi-autoencoders to solve the vanishing information problem in multi-layered neural networks, *Applied Intelligence* 49 (2019) 2522–2545.
- [23] D. Balduzzi, M. Frean, L. Leary, J. Lewis, K. W.-D. Ma, B. McWilliams, The shattered gradients problem: If resnets are the answer, then what is the question?, in: *Proceedings of the 34th International Conference on Machine Learning-Volume 70*, JMLR. org, 2017, pp. 342–350.
- [24] S. Hochreiter, J. Schmidhuber, Long short-term memory, *Neural computation* 9 (1997) 1735–1780.
- [25] G. Patrini, A. Rozza, A. Krishna Menon, R. Nock, L. Qu, Making deep neural networks robust to label noise: A loss correction approach, in: *Proceedings of the IEEE Conference on Computer Vision and Pattern Recognition*, 2017, pp. 1944–1952.
- [26] J. Howard, *imagenette*, 2019. URL: <https://github.com/fastai/imagenette/>.
- [27] A. Krizhevsky, V. Nair, G. Hinton, *Cifar-10*, 2009. URL: <http://www.cs.toronto.edu/~kriz/cifar.html>.
- [28] Y. LeCun, C. Cortes, *MNIST handwritten digit database*, <http://yann.lecun.com/exdb/mnist/>, 2010. URL: <http://yann.lecun.com/exdb/mnist/>.
- [29] Y. Netzer, T. Wang, A. Coates, A. Bissacco, B. Wu, A. Y. Ng, Reading digits in natural images with unsupervised feature learning, 2011.

- [30] L. Liu, H. Jiang, P. He, W. Chen, X. Liu, J. Gao, J. Han, On the variance of the adaptive learning rate and beyond, in: Proceedings of the Eighth International Conference on Learning Representations (ICLR 2020), 2020.
- [31] M. Zhang, J. Lucas, J. Ba, G. E. Hinton, Lookahead optimizer: k steps forward, 1 step back, in: Advances in Neural Information Processing Systems, 2019, pp. 9593–9604.
- [32] M. Abadi, A. Agarwal, P. Barham, E. Brevdo, Z. Chen, C. Citro, G. S. Corrado, A. Davis, J. Dean, M. Devin, S. Ghemawat, I. Goodfellow, A. Harp, G. Irving, M. Isard, Y. Jia, R. Jozefowicz, L. Kaiser, M. Kudlur, J. Levenberg, D. Mané, R. Monga, S. Moore, D. Murray, C. Olah, M. Schuster, J. Shlens, B. Steiner, I. Sutskever, K. Talwar, P. Tucker, V. Vanhoucke, V. Vasudevan, F. Viégas, O. Vinyals, P. Warden, M. Wattenberg, M. Wicke, Y. Yu, X. Zheng, TensorFlow: Large-scale machine learning on heterogeneous systems, 2015. URL: <https://www.tensorflow.org/>, software available from tensorflow.org.
- [33] D. Peer, S. Stabinger, A. Rodríguez-Sánchez, conflicting_bundle.py - a python module to identify problematic layers in deep neural networks, Software Impacts 7 (2021) 100053.
- [34] K. He, X. Zhang, S. Ren, J. Sun, Identity mappings in deep residual networks, in: European conference on computer vision, Springer, 2016, pp. 630–645.
- [35] A. Zaemzadeh, N. Rahnavard, M. Shah, Norm-preservation: Why residual networks can become extremely deep?, IEEE Transactions on Pattern Analysis and Machine Intelligence (2020).